Modulation of Antimicrobial Peptide Potency in Stressed Lipid Bilayers

Valeria Losasso,[1,*] Ya-Wen Hsiao,[1] Fausto Martelli,[2] Martyn D. Winn,[1] and Jason Crain[2,3,†]
[1]Daresbury Laboratory, STFC, Daresbury, Warrington, England WA4 4AD, United Kingdom
[2]IBM Research, Hartree Centre, Daresbury, England WA4 4AD, United Kingdom
[3]Dept. of Biochemistry, University of Oxford, South Parks Road, Oxford, OX1 3QU, England

(Received 21 January 2019; published 24 May 2019)

It is shown that the tendency of an archetypal antimicrobial peptide to insert into and perforate a simple lipid bilayer is strongly modulated by tensile stress in the membrane. The results, obtained through molecular dynamics simulations, have been demonstrated with several lipid compositions and appear to be general, although quantitative details differ. The findings imply that the potency of antimicrobial peptides may not be a purely intrinsic chemical property and, instead, depends on the mechanical state of the target membrane.

DOI: 10.1103/PhysRevLett.122.208103

Biological cells are routinely exposed to a wide variety of mechanical forces that produce stress on the plasma membrane. These arise from interactions with the environment, between cells, and with the extracellular matrix, leading to sophisticated feedback mechanisms between membrane tension and cellular processes: Mechanical stimuli at the cell periphery induce changes in gene expression [1,2] and affect exo- or endocytosis, motility, fusion [3], and aspects of vesicle dynamics [4]. Focal adhesions have been found to show complex mechanosensitivity [5,6], and recent work has elucidated the effects of mechanical tension on the specification and expansion of stem cells during organ generation [7]. At the molecular scale, certain ion channels in the plasma membrane (e.g., the bacterial membrane protein MscL, or the eukaryotic K2P potassium channels) can be mechanically gated [8–10], acting as exquisitely sensitive force detectors over a wide dynamic range from just above thermal noise to near the lytic tension limit of the bilayer [2]. Here, the gating mechanism is thought to involve a conformational change in the channel protein triggered by tension applied to the cell membrane [11,12]. Mechanosensitive channels are critical for bacteria to respond to changes in osmotic pressure [13,14]. Observation of mechanical gating in reconstituted membranes supports the view that the mechanism depends only on membrane tension rather than cytoskeletal effects or signalling pathways [12].

Sufficiently high mechanical stress leads to spontaneous pore formation and compromises membrane integrity, as has been well studied for model vesicles [15]. Such poration events can also be induced chemically and are a fundamental aspect of many natural and cytotoxic processes: Host defense peptides, for example, are conserved components of the innate immune systems of all organisms. They are believed to function by perforating or permeabilizing the membranes of pathogenic bacteria, although the molecular mechanisms involved remain under active investigation [16,17]. Membrane disruption by antimicrobial peptides (AMPs) is thought to induce leakage of ions and metabolites, and to reduce the transmembrane potential, resulting in impaired osmotic regulation and eventual membrane rupture.

The extent to which chemically induced cell poration and lysis can be influenced by mechanical stress is unexplored and is the subject of the present Letter.

The simplest molecular model of a cellular membrane is that of a lamellar lipid bilayer with self-assembly driven by hydrophobic organization. As a two-dimensional fluid, bilayers have a high elastic modulus but low shear modulus [18]. According to classical nucleation theory, the free energy required to form a circular pore of radius r in a bilayer at tension λ is decomposable into competing edge and surface terms according to $\Delta G(r) = 2\pi\sigma r - \pi r^2\lambda$. In the first term, σ is a line tension that determines the energy penalty for supporting the pore boundary, whereas the second term is the elastic energy reduction due to the pore [19]. This simple continuum description encapsulates the central idea of competing forces, but it fails to provide a sufficiently detailed description when the pore size is comparable to molecular dimensions, and where structural rearrangement of the lipid polar groups occurs [20]. Moreover, it does not allow for metastable prepores, which are thought to occur in real membranes; very recently, the conditions under which small pores exist as metastable defects in tensionless membranes have been proposed [21].

Thousands of membrane-disrupting peptides have been discovered in nature, which vary in sequence length, net charge, secondary structure, and other physical properties [22]. We will consider here an archetypal peptide of the cecropin family. The antibacterial spectrum of cecropins is broad, and activity is understood to arise from membrane permeation rather than by receptor-mediated recognition [23]. The cecropin B (CecB) variant possesses the highest activity in the family [24]. In the membrane environment,

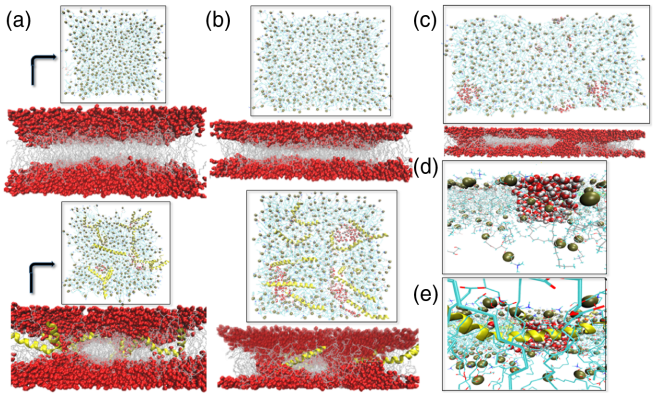

FIG. 1. Snapshots from MD simulations (top and side views) of a 3:1 DLPC:DLPG membrane without peptides (top) and with CecB peptides (bottom): (a) after 500 ns, no tensile stress applied; (b) after 50 ns, $\lambda = 20$ dyn/cm; and (c) after 150 ns of increasing stress, 20-50-60 dyn/cm. Water is shown as red spheres, peptides in yellow, and lipids as gray sticks with head groups as spheres. (d) Side view of the pore formed without peptides. (e) Side view of the pore formed with peptides.

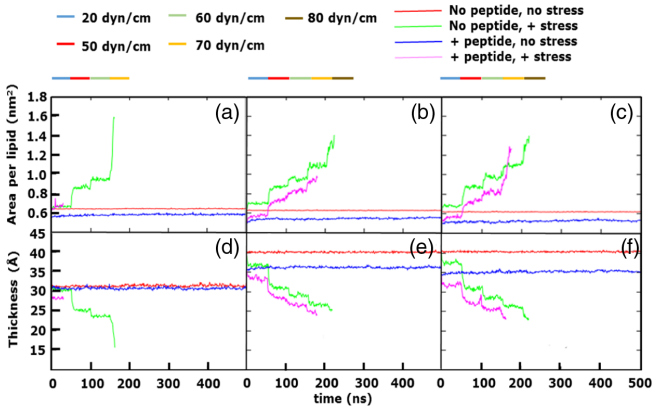

FIG. 2. (a)–(c): Area per lipid over time (left to right: DLPC:DLPG, POPC, and POPC:POPG). (d)–(f): Membrane thickness over time (left to right: DLPC:DLPG, POPC, and POPC:POPG). For each lipid composition, these quantities are plotted with or without peptide present, and with/without applied stress. The colored bars above each graph show the time profile of the applied stress.

the CecB structure comprises two α helices linked by a hinge—a motif shared with several other antimicrobial peptides.

We explore the extent to which the tendency of CecB to induce metastable prepores in simple lipid bilayers is influenced by the mechanical state of the membrane. Unbiased, atomistic molecular dynamics (MD) simulations using different lipid compositions are used to determine the structure of the peptide-membrane complexes. We also perform calculations of the potential of mean force (PMF) for a key mode of peptide insertion, computed using the adaptive biasing force (ABF) method implemented in the NAMD software [25].

We use a 3:1 DLPC:DLPG lipid mixture as an example of a short chain, saturated, negatively charged membrane composition, which we have used in a recent study of peptide cooperativity [24]. We also present results for other lipid compositions including POPC (long chain, unsaturated, neutral), 3:1 POPC-POPG (long chain, unsaturated, negatively charged), and 3:1 DSPC-DSPG (long chain, saturated, negatively charged). We consider systems without peptide or with ten copies of CecB, and either unstressed or with a stepwise increase of external tensile stress λ [26], achieved by using the surfaceTensionTarget module in NAMD [27]. All unbiased simulations were run until the appearance of the first pore or up to 500 ns otherwise, as well as in two independent runs to achieve better sampling. Table 1 in the Supplemental Material [26] shows a summary of the results.

Figure 1 displays example snapshots of MD simulations for DLPC:DLPG alone (top) and with 10 CecB peptides (bottom) initially placed at the water-lipid interface. With no external tension applied, neither system exhibits poration, although membrane defects can be observed when peptides are present [Fig. 1(a), bottom]. This is in agreement with previous observations of AMP penetration into membranes without forming transmembrane channels [37]. Although CecB in unstressed systems does not form pores, poration is observed (see Supplemental Material Sec. III. B [26] and Fig. S1 for its definition [38]) after a few nanoseconds when a tensile stress of only 20 dyn/cm is applied [Fig. 1(b), bottom; and Fig. 1(e)], which is in contrast to the membrane-only system (top). A notably higher tensile stress of 60 dyn/cm is required to perforate the membrane in the absence of CecB [Figs. 1(c) and 1(d); and Table 1 in the Supplemental Material [26]].

To characterize the physical effects of applied stress λ and the added peptides, we monitor the area per lipid (APL) and the bilayer thickness over the course of each simulation [37]. With no peptide present and no external tension, we find an average APL of 0.64 nm^2 and a thickness of 31.29 Å for DLPC:DLPG [Figs. 2(a) and 2(d)], 0.63 nm^2 and 40.1 Å for POPC [Figs. 2(b) and 2(e)], and 0.64 nm^2 and 41.78 Å for POPC:POPG [Figs. 2(c) and 2(f)]. DSPC:DSPG (0.64 nm^2 and 46 Å; Fig. S2) is found to display a gel phase (Fig. S3), which is in agreement with the experimental data [39,40] and with the overstabilization of ordered structures reported in the computational analysis in [41]. As a control, we have therefore run DSPC:DSPG simulations, also at a temperature of 368 K (i.e., 40 K above DSPC/DSPG transition temperature) for consistency with the other compositions (Fig. S4). The lower applied stress needed to perforate the membrane in the presence of CecB (60 vs 80 dyn/cm; see Table S2) is consistent with findings related to DLPC:DLPG, pure POPC, and POPC:POPG.

For all lipid compositions, the bilayer thickness decreases slightly in the presence of peptides and dramatically with increased tensile stress [Figs. 2(d)–2(f)]. The latter is clearly visible for the DLPC:DLPG system shown

in Fig. 1. The APL decreases with CecB, given the extra space required to fit it, but it increases as stress is applied [Figs. 2(a)–2(c)].

The curves in Fig. 2 for systems under stress terminate when poration occurs. The faster poration in the presence of peptides illustrated in Fig. 1 for the DLPC:DLPG membrane can be seen in Figs. 2(a) and 2(d). POPC and POPC:POPG systems show a similar trend, which is consistent over both independent simulations, with a $\lambda = 80$–90 dyn/cm required for poration in the absence of peptide, and only 70 dyn/cm in the presence of CecB (Figs. S5 and S6; Table S1). The higher applied stress needed as compared to DLPC:DLPG can be explained by the lower head-to-tail volume ratio of these lipids, which is in agreement with [21]. Unstressed simulations do not show any poration on the timescale of these simulations [Figs. S5(a) and S6(a)]. As noted above, at 310 K, the DSPC:DSPG bilayer shows a conformation typical of the gel phase. Consequently, tensile stress values required to perforate the membrane are notably higher as compared to the previous systems, and they are independent of CecB presence (Table S1, and Fig. S4).

As critical tensions depend strongly on the loading rate [42], it is worth noting that our loading rate is the same for all systems. A relation has been proposed between the rupture tension and the loading rate [43], which includes parameters associated with membrane composition. When applied on DOPC with a loading rate (1.4 mN/m/ns [44]) similar to ours (0.2 mN/m/ns), the calculated rupture tension is 85 mN/m, which is consistent with simulation values [44] and with our rupture tensions. Many other simulation studies find comparably high stress values to be required for poration across a variety of lipid compositions and force fields [42,45–51].

From the changes in APL as a function of λ reported in Fig. 2, it is possible to calculate the compressibility modulus K_A of our systems as $K_A = (d\lambda/d(\mathrm{APL}))\mathrm{APL}_0$, where APL_0 is the area per lipid at the free energy minimum [52]. This expression is valid only at equilibrium conditions; hence we use APL values for the system with no tension ($\lambda = 0$ dyn/cm) and the one with the lowest tension ($\lambda = 20$ dyn/cm). For our 424-lipid POPC-only system, with APLs of 62.6 and 69.8 Å^2, respectively, the resulting value of K_A (173.7 ± 21 dyn/cm) is very similar to the one (185 ± 18 dyn/cm) computationally derived for a 416-lipid POPC system [50], and within the range of experimental values reported for similar lipids [53]. The K_A value at this system size is instead overestimated if obtained from lipid density fluctuations, as observed in prior work [52].

We next perform simulations using the adaptive biasing force method aimed at estimating the free energy barrier to insertion for a single CecB peptide in 3:1 DLPC:DPLG, in the presence or absence of external tensile stress. We choose $\lambda = 50$ dyn/cm, which is higher than the value (20 dyn/cm) used with 10 peptides (Supplemental Material [26], Table 1), due to the lower peptide:lipid ratio [54]. The reaction

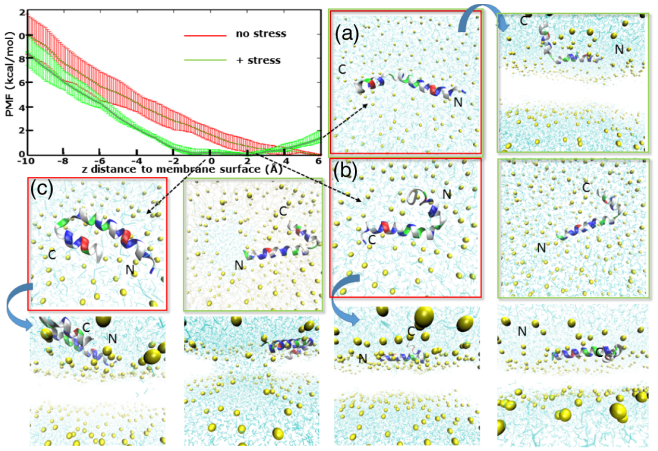

FIG. 3. The free energy of peptide insertion is changed qualitatively by the application of stress. PMF for CecB insertion into a tension-free DLPC:DLPG membrane (red) and one with $\lambda = 50$ dyn/cm (green). The origin of both lines is the membrane surface, calculated as the average of the upper leaflet phosphates position along the membrane normal. (a) Top and side views of the initial equilibrated system, which is the same for both curves, with the peptide N terminal 6 Å above the membrane surface ($d = 6$). (b) Peptide N terminal at $d = 2$. Top and side views with no stress applied are shown on the left, with applied stress on the right. (c) As for Fig. 3(b), with $d = 0$. CecB peptide is represented as a ribbon, with residues color coded as follows: red, negatively charged; blue, positively charged; green, polar; and white, hydrophobic.

coordinate for the calculation is the perpendicular distance (d) between the center of mass (COM) of the first three N-terminal residues of the peptide and the membrane surface, calculated as the z coordinate of the COM of the phosphorus atoms of the upper leaflet. In the ABF method, a biasing force facilitates the insertion of the peptide N terminal, which we take as the primary mode of action on the basis of the corresponding unbiased simulation with ten CecB peptides (Table S1, and Fig. S7), and it is consistent with previous work by Hsiao *et al.* [24]. We choose the membrane surface as the reference to allow for variation of the membrane thickness in the presence of tensile stress (Fig. 2). The calculation starts from the end of the equilibration phase, where the COM of the CecB N terminal lies 6 Å above the membrane surface (Fig. 3). Whereas the PMF curve for the unstressed membrane does not show clear minima or maxima (red in Fig. 3), the curve for the membrane under stress (green in Fig. 3) shows a broad minimum between $d = -2$ Å and $d = 2$ Å, implying a favorable insertion of the peptide into the region of the lipid headgroups.

In the system under stress, a pore appears at $d = 0$; see Fig. 3(c). The rearrangement of the system associated with pore formation may explain the broad free energy minimum in this region. For comparison, an unbiased control simulation with a single CecB peptide showed rapid pore formation and membrane disruption with $\lambda = 60$ dyn/cm.

This is only slightly greater than the applied stress of 50 dyn/cm used in the PMF calculation, but it is significantly greater than the 20 dyn/cm required in the presence of ten copies of CecB (Fig. 1). On the other hand, no pore appears while varying d in an unstressed system (Fig. 3, red boxes). Although the estimated ranges of the stressed and unstressed curves begin to overlap below $d = -6$ Å, they differ significantly over the first 5 Å below the membrane surface. This result suggests that the tensile stress plays a significant role in the early stages of penetration, but it may have less effect once the peptide is fully embedded into the membrane.

As outlined in [41], the increased APL under stress and the decreased bilayer thickness [Figs. 2 and S8(a)] cause a greater exposure of lipid tails to the solvent and to the adsorbed peptide. In the PMF simulation, we indeed observe a slight reduction of polar contacts between the peptide and the lipid headgroups [Fig. S8(b)], which is offset by a notably higher number of hydrophobic contacts with the lipid tails [Fig. S8(c)]. As expected, there is also an increase in hydrophobic contacts due to peptide insertion, but this change is smaller than that induced by applied stress.

Pore formation follows the disordered toroidal model [54], with the lipid headgroups reorienting towards the interior of the membrane to line the pore [Figs. 1(d) and 1(e)]. Pores are clearly distinguishable as local alterations of the z positions of headgroup phosphates, which are mirrored in the upper and lower leaflets of the bilayer [regions circled in Figs. 4(b) and 4(d)]. As a pore forms, water starts to penetrate and interact with lipid headgroups, forming a membrane perturbation [Fig. S1(a)], which then expands to a well defined pore [Figs. 1(d) and S1(b)]. When CecB is present, its charged N terminus immediately enters into the process by interacting with waters and lipid headgroups, whereas neutral side chains interact with exposed lipid tails, thus facilitating the poration [Figs. 1(e) and 4(e)].

It is possible to investigate precursor events in the poration process by analyzing the variation in the local lipid density. We quantify this by calculating the numbering of neighboring phosphate groups (closer than 5 Å) for each lipid phosphate group, and averaging over regions containing pore nucleation sites. Poration is preceded by a steep increase in the local phosphate density as the lipids cluster at the pore edges [see asterisks in Fig. 4(f)]. After pore formation, the local phosphate density decreases again, partly due to the presence of the pore itself. When peptides are present, these displace many lipid headgroups, again reducing the local density [Fig. 4(f); blue-cyan-pink lines]. Interestingly, the spike in local phosphate density suggests that the peptides respond to stabilize the pore rather than driving pore formation directly. The variation over time of the number of neighbors for each phosphate around the poration site is shown in the Supplemental Material (Movie S1) [26].

To conclude, we have used MD simulations and PMF calculations to elucidate the mechanism by which the ability of the antimicrobial peptide CecB to perforate

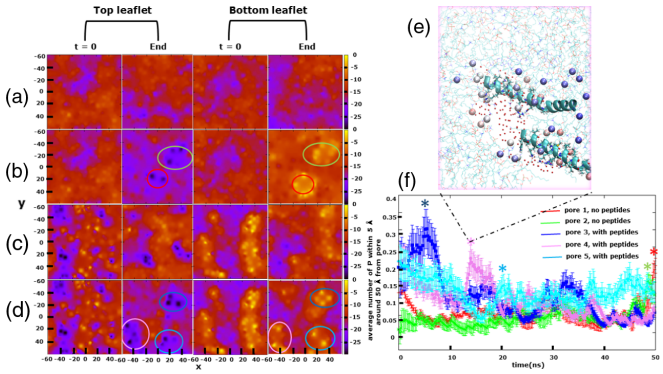

FIG. 4. Distribution of lipidic phosphate groups characterizing poration of a 3:1 DLPC:DLPG membrane. (a)–(d): Map of z coordinates for headgroup phosphates at $t = 0$ and at the end of the simulation for top and bottom leaflets. (a) Membrane only, no stress; (b) membrane only, $\lambda = 60$ dyn/cm; (c) membrane + CecB, no stress; and (d) membrane + CecB, $\lambda = 20$ dyn/cm. Circles indicate the location of a well-defined pore. (e) Snapshot of pore 4 (pink circle) formed by CecB with applied stress. Waters are represented as red dots, phosphorus atoms are colored by the z coordinate (blue to red = top to bottom). (f) Time course of the average number of close neighbors (P pairs closer than 5 Å) for all the phosphorus atoms within 50 Å from the pore nucleation site, over the last 50 ns of simulation. Asterisks [same colors as in Figs. 4(b) and 4(d)] indicate the point in time when the pore first appears.

different lipid compositions, which mimic bacterial membranes, is strongly modulated by tensile stress in the bilayer. CecB is a naturally occurring peptide with a broad spectrum of activity that shares several physical, chemical, and structural features with many other AMPs. Therefore, we believe that these results can be generalized to other AMP families.

For the systems studied here, the AMP CecB creates water or lipid interface perturbations but fails to form complete pores unless external stress is applied. This is consistent with a recent joint experimental and computational study of CecB and variants [55]. Conversely, poration can be induced through applied stress alone, but it is potentiated significantly by the presence of peptides. Estimated free energy profiles for peptide insertion show a qualitative change when stress is applied, and this can be rationalized in terms of specific peptide-lipid interactions. Finally, we have analyzed the distribution of lipidic phosphate groups that characterize the formation of disordered toroidal pores. Peptides act to stabilize the nascent pore, displacing some of the phosphate groups that line the pore.

It has been observed before that the assumptions of classical nucleation theory break down for small pores [20]. A key feature of applied stress (and, to a lesser extent, the addition of peptide) is to thin the membrane, and this is likely to reduce the line tension of any pore formed. A knowledge of the physical response of biological bilayers, as shown in Fig. 2, may help to predict the

stability of membranes. Nevertheless, line tension is also reduced by chemical factors, such as the rearrangement of lipid headgroups and the positioning of peptides [56]; and it is difficult to quantify this without a molecular understanding of the processes involved.

Extra stress leading to membrane expansion can be present in several biological systems, including bacterial cells and laboratory-prepared unilamellar vesicles [57]. Earlier studies [41,58] suggested that tension could have an effect on the action of AMPs, and the work presented here confirms this and provides a mechanistic rationale. A further understanding of the impact of the mechanical state of the membrane on antimicrobial peptides' potency with better mimics of bacterial membranes, inclusions of cardiolipins, is required to elucidate the mechanisms of bacterial drug resistance that develop through changes in lipid composition [59].

This work was supported by the STFC Hartree Centre's Innovation Return on Research program, funded by the Department for Business, Energy and Industrial Strategy. The STFC Hartree Centre is a research collaboratory in association with IBM providing High Performance Computing platforms funded by the UK's investment in e-Infrastructure.

*valeria.losasso@stfc.ac.uk
†Jason.Crain@ibm.com

[1] R. Bainer and V. Weaver, Strength under tension, Science **341**, 965 (2013).
[2] A. Diz-Muoz, D. A. Fletcher, and O. D. Weiner, Use the force: membrane tension as an organizer of cell shape and motility, Trends Cell Biol. **23**, 47 (2013).
[3] A. Grafmüller, J. Shillcock, and R. Lipowsky, Pathway of Membrane Fusion with Two Tension-Dependent Energy Barriers, Phys. Rev. Lett. **98**, 218101 (2007).
[4] W. W. Ahmed and T. A. Saif, Active transport of vesicles in neurons is modulated by mechanical tension, Sci. Rep. **4**, 4481 (2014).
[5] C. Grashoff, B. D. Hoffman, M. D. Brenner, R. Zhou, M. Parsons, M. T. Yang, M. A. McLean, S. G. Sligar, C. S. Chen, T. Ha, and M. A. Schwartz, Measuring mechanical tension across vinculin reveals regulation of focal adhesion dynamics, Nature (London) **466**, 263 (2010).
[6] B. D. Matthews, D. R. Overby, R. Mannix, and D. E. Ingber, Cellular adaptation to mechanical stress: role of integrins, Rho, cytoskeletal tension and mechanosensitive ion channels, J. Cell Sci. **119**, 508 (2006).
[7] K. H. Vining and D. J. Mooney, Mechanical forces direct stem cell behaviour in development and regeneration, Nat. Rev. Mol. Cell Biol. **18**, 728 (2017).
[8] O. P. Hamill and B. Martinac, Molecular basis of mechanotransduction in living cells, Physiol. Rev. **81**, 685 (2001).
[9] S. Ranade, R. Syeda, and A. Patapoutian, Mechanically activated ion channels, Neuron **87**, 1162 (2015).
[10] A. Anishkin and C. Kung, Stiffened lipid platforms at molecular force foci, Proc. Natl. Acad. Sci. U.S.A. **110**, 4886 (2013).
[11] D. J. Bonthuis and R. Golestanian, Mechanosensitive Channel Activation by Diffusio-Osmotic Force, Phys. Rev. Lett. **113**, 148101 (2014).
[12] M. S. Turner and P. Sens, Gating-by-Tilt of Mechanically Sensitive Membrane Channels, Phys. Rev. Lett. **93**, 118103 (2004).
[13] T. Walton, C. Idigo, N. Herrera, and D. Rees, MscL: channeling membrane tension, Pflugers Arch. Eur. J. Physiol. **467**, 15 (2015).
[14] U. Cetiner, I. Rowe, A. Schams, C. Mayhew, D. Rubin, A. Anishkin, and S. Sukharev, Tension-activated channels in the mechanism of osmotic fitness in Pseudomonas aeruginosa, J. Gen. Physiol. **149**, 595 (2017).
[15] M. Chabanon, J. C. Ho, B. Liedberg, A. N. Parikh, and P. Rangamani, Pulsatile lipid vesicles under osmotic stress, Biophys. J. **112**, 1682 (2017).
[16] P. D. Rakowska, H. Jiang, S. Ray, A. Pyne, B. Lamarre, M. Carr, P. J. Judge, J. Ravi, U. I. M. Gerling, B. Koksch, G. J. Martyna, B. W. Hoogenboom, A. Watts, J. Crain, C. R. M. Grovenor, and M. G. Ryadnov, Nanoscale imaging reveals laterally expanding antimicrobial pores in lipid bilayers, Proc. Natl. Acad. Sci. U.S.A. **110**, 8918 (2013).
[17] L. Chen, X. Li, L. Gao, and W. Fang, Theoretical insight into the relationship between the structures of antimicrobial peptides and their actions on bacterial membranes, J. Phys. Chem. B **119**, 850 (2015).
[18] J. Dai and M. Sheetz, Chapter 9 cell membrane mechanics, Methods Cell Biol. **55**, 157 (1997).
[19] H. W. Huang, F.-Y. Chen, and M.-T. Lee, Molecular Mechanism of Peptide-Induced Pores in Membranes, Phys. Rev. Lett. **92**, 198304 (2004).
[20] C. L. Ting, D. Appelö, and Z. G. Wang, Minimum Energy Path to Membrane Pore Formation and Rupture, Phys. Rev. Lett. **106**, 168101 (2011).
[21] C. L. Ting, N. Awasthi, M. Müller, and J. S. Hub, Metastable Prepores in Tension-Free Lipid Bilayers, Phys. Rev. Lett. **120**, 128103 (2018).
[22] Y.-H. Li, Z. Zhong, W.-P. Zhang, and P. Qian, Discovery of cationic nonribosomal peptides as Gram-negative antibiotics through global genome mining, Nat. Commun. **9**, 3273 (2018).
[23] E. Gazit, W.-J. Lee, P. T. Brey, and Y. Shai, Mode of action of the antibacterial Cecropin B2: A spectrofluorometric study, Biochemistry **33**, 10681 (1994).
[24] Y.-W. Hsiao, M. Hedström, V. Losasso, S. Metz, J. Crain, and M. Winn, Cooperative modes of action of antimicrobial peptides characterized with atomistic simulations: A study on Cecropin B, J. Phys. Chem. B **122**, 5908 (2018).
[25] J. Hénin, G. Fiorin, C. Chipot, and M. L. Klein, Exploring multidimensional free energy landscapes using time-dependent biases on collective variables, J. Chem. Theory Comput. **6**, 35 (2010).
[26] See Supplemental Material at http://link.aps.org/supplemental/10.1103/PhysRevLett.122.208103 for details on the methods used, which include Refs. [27–36].
[27] J. C. Phillips, R. Braun, W. Wang, J. Gumbart, E. Tajkhorshid, E. Villa, C. Chipot, R. D. Skeel, L. Kale, and K. Schulten, Scalable molecular dynamics with NAMD, J. Comput. Chem. **26**, 1781 (2005).

[28] S. Jo, T. Kim, V. Iyer, and W. Im, CHARMM-GUI: A web-based graphical user interface for CHARMM, J. Comput. Chem. **29**, 1859 (2008).
[29] Schrödinger, LLC, The PyMOL Molecular Graphics System, Version 1.8.
[30] W. Humphrey, A. Dalke, and K. Schulten, VMD: Visual molecular dynamics, J. Mol. Graphics **14**, 33 (1996).
[31] J. B. Klauda, R. M. Venable, J. A. Freites, J. W. O'Connor, D. J. Tobias, C. Mondragon-Ramirez, I. Vorobyov, A. D. MacKerell, and R. W. Pastor, Update of the CHARMM all-atom additive force field for lipids: Validation on six lipid types, J. Phys. Chem. B **114**, 7830 (2010).
[32] A. D. MacKerell *et al.*, All-atom empirical potential for molecular modeling and dynamics studies of proteins, J. Phys. Chem. B **102**, 3586 (1998).
[33] W. L. Jorgensen, J. Chandrasekhar, J. D. Madura, R. W. Impey, and M. L. Klein, Comparison of simple potential functions for simulating liquid water, J. Chem. Phys. **79**, 926 (1983).
[34] U. Essmann, L. Perera, M. L. Berkowitz, T. Darden, H. Lee, and L. G. Pedersen, Comparison of simple potential functions for simulating liquid water, J. Chem. Phys. **103**, 8577 (1995).
[35] S. Buchoux, FATSLiM: a fast and robust software to analyze MD simulations of membranes, Bioinformatics **33**, 133 (2017).
[36] R. Guixa-Gonzalez, I. Rodriguez-Espigares, J. M. Ramirez-Anguita, J. Carrio-Gaspar, H. Martinez-Seara, T. Giorgino, and J. Selent, MEMBPLUGIN: studying membrane complexity in VMD, Bioinformatics **30**, 1478 (2014).
[37] J. B. Ulmschneider, Charged antimicrobial peptides can translocate across membranes without forming channel-like pores, Biophys. J. **113**, 73 (2017).
[38] M. Nishizawa and K. Nishizawa, Molecular dynamics simulation analysis of membrane defects and pore propensity of hemifusion diaphragms, Biophys. J. **104**, 1038 (2013).
[39] N. Kucerka, M. Nieh, and J. Katsaras, Fluid phase lipid areas and bilayer thicknesses of commonly used phosphatidylcholines as a function of temperature, Biochim. Biophys. Acta Biomembr. **1808**, 2761 (2011).
[40] J. Pan, F. Heberle, S. Tristram-Nagle, M. Szymanski, M. Koepfinger, N. Kucerka, and J. Katsaras, Molecular structures of fluid phase phosphatidylglycerol bilayers as determined by small angle neutron and X-ray scattering, Biochim. Biophys. Acta **1818**, 2135 (2012).
[41] K. Reid, C. Davis, R. Dyer, and J. Kindt, Molecular structures of fluid phase phosphatidylglycerol bilayers as determined by small angle neutron and X-ray scattering, Biochim. Biophys. Acta Biomembr. **1860**, 792 (2018).
[42] D. Tieleman, H. Leontiadou, A. Mark, and S. Marrink, Simulation of pore formation in lipid bilayers by mechanical stress and electric fields, J. Am. Chem. Soc. **125**, 6382 (2003).
[43] E. Evans, V. Heinrich, F. Ludwig, and W. Rawicz, Dynamic tension spectroscopy and strength of biomembranes, Biophys. J. **85**, 2342 (2003).
[44] M. Tomasini, C. Rinaldi, and M. Tomassone, Molecular dynamics simulations of rupture in lipid bilayers, Experimental biology and medicine **235**, 181 (2010).
[45] A. Reddy, D. Warshaviak, and M. Chachisvillis, Effect of membrane tension on the physical properties of DOPC lipid bilayer membrane, Biochim. Biophys. Acta Biomembr. **1818**, 2271 (2012).
[46] J. Xie, G. Ding, and M. Karttunen, Molecular dynamics simulations of lipid membranes with lateral force: Rupture and dynamic properties, Biochim. Biophys. Acta Biomembr. **1838**, 994 (2014).
[47] H. Leontiadou, A. E. Mark, and S. J. Marrink, Molecular dynamics simulations of hydrophilic pores in lipid bilayers, Biophys. J. **86**, 2156 (2004).
[48] E. M. Houang, F. S. Bates, Y. Sham, and J. Metzger, All-atom molecular dynamics-based analysis of membrane-stabilizing copolymer interactions with lipid bilayers probed under constant surface tensions, J. Phys. Chem. **121**, 10657 (2004).
[49] H. Leontiadou, A. E. Mark, and S. J. Marrink, Ion transport across transmembrane pores, Biophys. J. **92**, 4209 (2007).
[50] M. Doktorova, M. V. LeVine, G. Khelashvili, and H. Weinstein, A new computational method for membrane compressibility: bilayer mechanical thickness revisited, Biophys. J. **116**, 487 (2019).
[51] D. Sun, J. Forsman, and C. Woodward, Multistep molecular dynamics simulations identify the highly cooperative activity of melittin in recognizing and stabilizing membrane pores, Langmuir **31**, 9388 (2015).
[52] R. Feller and R. Pastor, Constant surface tension simulations of lipid bilayers: The sensitivity of surface areas and compressibilities, J. Chem. Phys. **111**, 1281 (1999).
[53] W. Rawicz, K. C. Olbrich, T. McIntosh, D. Needham, and E. Evans, Effect of chain length and unsaturation on elasticity of lipid bilayers, effect of chain length and unsaturation on elasticity of lipid bilayers, Biophys. J. **79**, 328 (2000).
[54] D. Sengupta, H. Leontiadou, A. Mark, and S. Marrink, Toroidal pores formed by antimicrobial peptides show significant disorder, Biochim. Biophys. Acta Biomembr. **1778**, 792 (2008).
[55] M.-P. Pfeil, A. L. B. Pyne, V. Losasso, J. Ravi, B. Lamarre, N. Faruqui, H. Alkassem, K. Hammond, P. J. Judge, M. Winn, G. J. Martyna, J. Crain, A. Watts, B. W. Hoogenboom, and M. G. Ryadnov, Tuneable poration: host defense peptides as sequence probes for antimicrobial mechanisms, Sci. Rep. **8**, 14926 (2018).
[56] J. Henderson, A. Waring, and K. Separovic, and F. Lee, Antimicrobial peptides share a common interaction driven by membrane line tension reduction, Biophys. J. **111**, 2176 (2016).
[57] Y. Sun, T.-L. Sun, and H. W. Huang, Physical properties of Escherichia coli spheroplast membranes, Biophys. J. **107**, 2082 (2014).
[58] J. E. Faust, P.-Y. Yang, and H. W. Huang, Action of antimicrobial peptides on bacterial and lipid membranes: A direct comparison, Biophys. J. **112**, 1663 (2017).
[59] R. M. Epand and R. F. Epand, Lipid domains in bacterial membranes and the action of antimicrobial agents, Biochim. Biophys. Acta Biomembr. **1788**, 289 (2009).